Published in final edited form as:
Nanotechnology. 2009 September 2; 20(35): 355102. doi:10.1088/0957-4484/20/35/355102.

Enhanced stem cell tracking *via* electrostatically assembled fluorescent SPION-peptide complexes

Jae-Ho Lee[1,3,6], **Melissa A. Smith**[1], **Wei Liu**[1,4], **Eric M. Gold**[1], **Bobbi Lewis**[1], **Ho-Taek Song**[1,5], and **Joseph A. Frank**[1,2]

Jae-Ho Lee: leejaeho@mail.nih.gov; Melissa A. Smith: ; Wei Liu: wei.liu_1@philips.com; Eric M. Gold: ; Bobbi Lewis: ; Ho-Taek Song: hotsong@yuhs.ac; Joseph A. Frank: jafrank@helix.nih.gov

[1]Frank Laboratory, Radiology and Imaging Sciences, Clinical Center, National Institute of Biomedical Imaging and Bioengineering, National Institutes of Health, Bethesda, MD 20892-1074, USA

[2]Intramural Research Program, National Institute of Biomedical Imaging and Bioengineering, National Institutes of Health, Bethesda, MD 20892-1074, USA

[3]CCR Nanobiology Program, Membrane Structure and Function Section, National Cancer Institute of Health at Frederick, Frederick, MD 21702-1201

[4]Philips Research North America, Briarcliff Manor, NY 10510, USA

[5]Department of Radiology, Yonsei University College of Medicine, Seoul 120-752, Korea

Abstract

For cellular MRI there is a need to label cells with superparamagnetic iron oxide nanoparticles (SPION) that have multiple imaging moieties that are nontoxic and have increased NMR relaxation properties to improve the detection and tracking of therapeutic cells. Although increases in the relaxation properties of SPION have been accomplished, detection of tagged cells is limited by either poor cell labeling efficiency or low intracellular iron content. A strategy *via* a complex formation with transfection agents to overcome these obstacles has been reported. In this paper, we report a complex formation between negatively charged fluorescent mono-disperse SPION and positively charged peptides and use the complex formation to improve the MR properties of labeled stem cells. As a result, labeled stem cells exhibited strong fluorescent signal and enhanced T2* weighted MR imaging *in vitro* and *in vivo* in a flank tumor model.

Keywords

fluorescent SPION; stem cell labeling; multimodal imaging; SPION-peptide complex

1. Introduction

There is increasing interest in using cellular therapies to treat diseases. Moreover, using cells as delivery vehicles for nanotherapeutics has prompted the need for developing methods to track cells noninvasively within the body. Various contrast agents and reporter gene constructs have been used to label cells so that they can be tracked using optical or bioluminescent imaging, nuclear medicine approaches or magnetic resonance imaging (MRI) techniques [1–

6Author to whom any correspondence should be addressed.

Classification numbers : Biology and Medicine PACS section 87, MSC 92C50 Submitted to Nanotechnology

3]. For MRI, endocytosis of superparamagnetic iron oxide nanoparticles (SPION) by cells has been developed [4–7], including a simple cell labeling method that relies on electrostatically assembled complexes [8,9]. However, there is a need to label cells with multimodal SPION that have improved magnetic properties in order to track tagged cells in target tissues [8].

For biomedical applications, superparamagnetic nanoparticles should be water-soluble, biocompatible, and stable *in vitro* and *in vivo*. Multimodal functionality such as the addition of a fluorescent probe to the SPION provides an added dimension to the contrast agent providing the ability for imaging-pathological correlation [10–15]. Improvements in the magnetic properties of SPION have been accomplished by producing monodisperse and highly crystalline iron oxide nanoparticles through high-temperature decomposition approaches [16–18], and by controlling the clustering of magnetic nanoparticles [19]. Although several approaches have been tried to effectively label cells with monodisperse and highly crystalline SPION, the incorporation of these agents into cells has been shown to be inefficient, thereby limiting their use in MRI cell trafficking studies [12]. Our previous findings demonstrated that anionic SPION are not endocytosed in high concentration by nonphagocytic cells [8]. By mixing different ratios of SPION with transfection agents it is possible to magnetically label stem cells and other non-phagocytic cells over a range of complexation conditions that are assembled electrostatically [14,20].

In this study, we systematically investigated a complex formation of negatively charged fluorescent (FL) SPION and positively charged peptide, and derived a general complex theory to predict the complex formation. By conjugating Texas Red (Texas) dextran to SPION, we labeled stem cells *via* the complex formation and compared the labeling efficiency of these fluorescent SPION agents. We also evaluated multimodal nanoparticle labeled stem cells by fluorescent microscopy and MRI. Furthermore, we tracked labeled human mesenchymal stem cells in flank tumor nude mouse model by *in vivo* fluorescent and MR imaging.

2. Materials and methods

2.1. Reagents and cell lines

All chemicals were purchased from Sigma-Aldrich unless specified otherwise. Texas Red® was supplied as lysine fixable dextran conjugates (molecular weight 3kDa, Invitrogen, Carlsbad, CA). Human Bone Marrow Stromal Cells, also known as Human Mesenchymal Stem Cells (hMSC) and human cervical carcinoma (HeLa) cells (CCL-2, ATCC, Manassas, VA) were used for cell labeling. hMSC were obtained from volunteers undergoing bone marrow biopsy under institutional review board-approved procedures, in accordance with NIH regulations governing the use of human subjects.

2.2. Synthesis of Fluorescent SPION

Fluorescent SPION was synthesized by conjugating fixable fluorescent dextran to various SPION as described previously [14]. High temperature synthesized iron oxide nanoparticles (HTIO) coated by carboxylic acid functionalized biocompatible amphiphilic triblock copolymer (Ocean Nanotech, Fayetteville, AR, core size 10 nm (HTIO10) or 15 nm (HTIO15)), were first modified with 2mM EDC (Pierce, Rockford, IL) and 5mM Sulfo-NHS (Pierce, Rockford, IL). After reaction, the amine-reactive Sulfo-NHS ester functionalized SPION was purified by running the solution through a PD 10 column (GE Healthcare, Piscataway, NJ), filled with Sephadex G-25, twice. Next, fixable Texas Red® dextran to the amine-reactive Sulfo-NHS ester functionalized SPION (0.5mg dye/1mg Fe) was introduced and allowed to react overnight at 4°C in the dark room. The following day the fluorescent dye conjugated SPION solution was passed four times through PD 10 columns or until the column showed a clear separation. Fluorescent dye conjugation efficiency (dye/iron) was obtained from the

absorbance of maximum peak of dye (Texas Red® 595nm) using the extinction coefficient (Texas Red® 80000 $M^{-1}cm^{-1}$).

2.3. Biophysical properties of nanoparticles and complexes

The surface charge of nanoparticles or of complexes was measured by a zeta potential (ZP) analyzer (ZetaPALS, Brookhaven Instruments, Long Island, NY), reported in millivolts (mV). Nuclear Magnetic Resonance (NMR) relaxometry was performed to determine relaxation parameters (i.e., $1/T_1$, and $1/T_2$) of nanoparticles on custom designed units described previously [21]. The hydrodynamic diameter was analyzed by dynamic light scattering (ZetaPALS, Brookhaven Instruments, Long Island, NY). Each sample was measured three times and the average diameter was reported.

2.4. Formation of FL SPION-protamine sulfate (FL SPION-Pro) complex for cell labeling

FL SPION-Pro complexes were prepared as previously reported [8,14] and cells were labeled at optimum complexation conditions for each SPION. SPION, 100 μg/ml in suspension, were added to a tube containing GIBCO® serum-free RPMI 1640 cell culture medium (Invitrogen, 11875) and mixed with protamine sulfate at various concentrations (e.g., for FE-Pro complex 6 μg/ml protamine sulfate [10 mg/ml, molecular weight 4.2kDa, American Pharmaceuticals Partner, Schaumburg, IL]). The complex solutions of FL SPION-Pro were then used to label cells that were grown in 6-well plates at density of 2×10^6 cells/ml. For hMSC labeling, two to three hours following initial incubation with SPION solution, fresh α-MEM media with additives was added to each well at a predetermined amount to reach a final volume of media to contrast agent of 2 ml per well (i.e., iron concentration 50 μg/ml).

2.5. Cellular viability and proliferation capacity

Cell viability was determined by a trypan blue exclusion test. Cell proliferation capacity was determined by t h e M T S (3-[4,5-dimethylthiazol-2-y1]-5-[3-carboxymethoxypheny1]-2-[4-sulfopheny1]-2H-tetrazolium, inner salt) cell proliferation assay (CellTiter 96® Aqueous One Solution, Promega, Madison, WI). FE-Pro labeled, Texas HTIO-Pro labeled and unlabeled control cells were plated in triplicate in a 96-well plate at cell density of 5000cells/100μl. Cell growth was measured at 1, 24, and 72 hours after plating by adding 20 μL of MTS reagent and incubating at 37°C for an hour. Proliferation and viability was recorded by measuring the absorbance at 490 nm using UV-visible spectrophotometer (UV-1601, Shimadzu, Japan).

2.6. Determination of mean iron concentration per cell

Iron concentration was assayed by a variable-field relaxometer (Southwest Research Institute, San Antonio, TX) and UV-visible spectrophotometer as previously described [4,14]. Measurement standards were prepared by serially diluting 500 μl of the Feridex standard (con. 0.174mg/ml) into 500 μl of deionized water six times. 500 μl of 10N hydrochloric acid was then added to each dilution. The SPION samples were prepared by adding 500 μL of 10N hydrochloric acid to 500 μl of FE-Pro labeled, Texas HTIO-Pro labeled and control cells, diluted to a concentration of 1×10^5 cells/ml in deionized water, respectively. The samples incubated overnight to allow the cells to digest. The NMR relaxation rate $1/T_2$ (s^{-1}) was measured at 1.0 T (42.6 MHz) at 23°C.

2.7. Histology

For microscopy, cells were washed with heparinized PBS (15 mg/ml), diluted to 720 cells/μl, and resuspended in Cytofix solution. Cytospin slides were fixed with 4% paraformaldehyde. For fluorescent microscopy, slides were then allowed to air dry, washed in distilled water in the dark, allowed to dry again and cover-slipped with VectaShield with DAPI (Vector Laboratories, Burlingame, CA). To minimize autofluorescence, exposure times were based on

the signal intensity from unlabeled control cells and fluorescent images were obtained using DAPI and Cy3 filters. Overlapping images were obtained by Z-stacks, an application provided by the software on the microscope. For light microscopy cytospin slides were stained with Prussian blue. Prussian blue stains were done on cytospin slides with a 30 minute incubation using a 1:1 ratio of 20% potassium ferrocyanide and 20% hydrochloric acid to detect the presence of SPION in cells. The slides were then washed with de-ionized water and counterstained with Nuclear Fast Red (Scytek, Logan, UT). The Prussian blue stained cytospin slides were evaluated for iron staining with a Zeiss microscope (Axioplan Imaging II; Zeiss, Oberkochen, Germany) at × 40/0.75 objective lens with Axiovision 4 software (Zeiss). SPION labeling efficiency was determined by using images of the Prussian blue stained FL SPION-Pro labeled cells captured by Axioplan Imaging II at 100× magnification using ×100/1.3 (oil) immersion objective lens. The images were imported into the Image J program of NIH to obtain cell counts of labeled versus unlabeled cells.

2.8. MRI at 3 Tesla

A phantom was made from a cylindrical glass tube, 6 cm in diameter, filled with distilled water. Plastic vials with FE-Pro labeled, Texas HTIO-Pro labeled or unlabeled cells were suspended in 1 ml 1% agarose gel. The sealed vials were embedded in the middle of the glass cylinder on a plastic rack. MRI was performed on a 3T clinical MR scanner (Acheiva, Philips Medical System, Best, The Netherlands) using a dedicated 7 cm solenoid receive only RF-coil (Philips Research Laboratories, Hamburg, Germany). The T^2* relaxation map was acquired using a multiple gradient echo sequence with 15 echoes: TR = 1400 ms, TE of the first echo= 3.6 ms, FA = 30° and inter echo step between consecutive echoes=2.8ms. All images were acquired with a field of view = 100 mm × 100 mm, data matrix = 256 × 256, slice thickness = 1 mm, and number of excitations = 2.

2.9. Detection limit of FL SPION by fluorescent imaging system

To determine the detection limit of several FL SPION by a multispectral imaging system (Maestro, CRI Inc., Woburn, MA), uniformly sliced chicken breast was used as a tissue phantom. The average slice thickness of each tissue section was approximately 2 mm. Equal amounts of FL SPION (50μg) were loaded on the top of a section. The iron concentration was determined before the experiment and the corresponding SPION solution was localized on the tissue section. The solution volume was controlled to keep FL SPION only on the surface. To minimize the fluorescent signal from the tissue, the area of dye loaded tissue section was smaller than the tissue sections. The slices of tissue at various thicknesses were covered in order to determine the ability to detect FL SPION (see results for details). Images were analyzed by using the spectral unmixing algorithms provided by the multispectral imaging system to separate auto-fluorescence from the desired fluorescent signal. The total signal intensity was measured for each sample at various depths from the surface of the phantom and normalized to tissues of same slice thickness with control SPION sample that was did not contain fluorochrome (see the supporting figure).

2.10. In vivo MR and fluorescent imaging of labeled stem cells

Athymic nude mice (nu/nu NCI Frederick, Maryland) were imaged under isofluorane anesthesia for all *in vivo* imaging studies and euthanized according to an approved animal care and use committee protocol at our institution. C6 glioma cells were subcutaneously implanted to both flanks of nude mice. Texas HTIO15-Pro labeled hMSC (10^6 cells) mixed with 10^6 unlabeled C6 glioma cells in phosphate buffered saline (200 μl) were injected subcutaneously into the right flank of mice. In the contralateral flank 10^6 FE-Pro labeled hMSC and 10^6 unlabeled C6 glioma 8 cells were injected subcutaneously. When the tumors reached approximately 1 cm in size (approximately 7 days post implantation), *in vivo* fluorescent

images were obtained using multispectral imaging system. 529 nm excitation band pass filter and 580 nm long pass emission filter were used. Images were analyzed by using the spectral unmixing algorithms to separate auto-fluorescence from the desired fluorescent signal of Texas Red.

Following optical imaging, *in vivo* MRI was performed on mice (n=3) with flank tumors on a 3T scanner (Achieva, Philips Medical System, Netherlands, B.V.) using a solenoid 4 cm radiofrequency receive only coil (Philips Research Laboratories, Germany). Physiological monitoring was performed with SAII MRI compatible unit (Small Animal Instruments Inc., Stony Brook, NY). The MR pulse sequences were as follows: T2-weighted (T2w) turbo spin echo (TSE) sequence, repetition time (TR)/ echo time (TE) = 5200/60 ms, turbo spin echo factor 12, number of average (NAV) 8, field of view (FOV) 50 mm, slice thickness 1 mm, matrix 224×256, reconstructed resolution 115×115 μm; and a T2* multi echo gradient sequence (T2*w), TR/effective TE = 4560/28 ms, 15 echos, flip angle 30°, NAV 2, FOV 50 mm, slice thickness 0.5 mm, matrix 176×256, reconstructed resolution 200×200 μm. The mice were euthanized and tumors were Prussian blue stained to detect iron-labeled cells. Differences between the various treatments were statistically tested using Student's t-test. P values of less than 0.05 were considered statistically significant.

2.11. Complex formation theory

Following relationships were derived for complex formation.

$$Z_p\,(\text{Zeta potential}) \sim \sigma\,(\text{surface charge density}) \tag{1}$$

$$\Gamma\,(\text{total charge per particle}) = \sigma \cdot (4\pi r^2) = k \cdot Z_p \cdot (4\pi r^2) \tag{2}$$

where r is the radius of particle and k is the constant.

Electrostatically assembled complexation occurs at neutral media condition. Therefore, total positive and total negative charges are the same in media.

$$N_- \cdot k_- \cdot Z_p^- \cdot (4\pi r_-^2) = N_+ \cdot k_+ \cdot Z_p^+ \cdot (4\pi r_+^2) \tag{3}$$

where N is the number of particle. Then, mass is correlated with radius.

$$m = N \cdot \rho \cdot \frac{4}{3} \cdot \pi r^3 \tag{4}$$

where ρ is the density. By putting equation 4 into equation 3,

$$\frac{3 \cdot m_- \cdot k_- \cdot Z_p^-}{\rho_- r_-} = \frac{3 \cdot m_+ \cdot k_+ \cdot Z_p^+}{\rho_+ r_+} \tag{5}$$

Equation 5 can be rearranged to equation 6.

$$m_+ = m_- \cdot \left(\frac{r_+ \cdot Z_p^-}{r_- \cdot Z_p^+}\right) \cdot \left(\frac{k_- \cdot \rho_+}{k_+ \cdot \rho_-}\right) \tag{6}$$

When $k_- \cdot \rho_+ / k_+ \cdot \rho_-$ is assumed to be constant at a neutral charge condition, the concentration of transfection agent amount, m_+ can be related by the following equation.

$$\begin{gathered} m_+ \sim m_- \cdot \left(\frac{r_+ \cdot Z_p^-}{r_- \cdot Z_p^+}\right) \text{ or} \\ m_+ \sim m_- \cdot \left(\frac{d_+ \cdot |Z_p^-|}{d_- \cdot Z_p^+}\right) = d_+ \cdot J \\ \text{where } J = \left(\frac{m_- \cdot |Z_p^-|}{d_- \cdot Z_p^+}\right) \end{gathered} \tag{7}$$

3. Results and discussion

3.1. Synthesis and physico-chemical properties of FL SPION

The conjugation efficiency for Texas HTIO15 and HTIO10 existing as a cluster formation was determined by a UV-visible spectrophotometer. The spectra of the Texas SPION in this study demonstrated a peak at 595nm, validating the conjugation of the fluorochrome dye to the SPION (Supporting Information). After surface modification, the zeta potentials of Texas HTIO15 and Texas HTIO10 were negative (Table 1). Table 1 summarizes the physico-chemical properties of the SPION contrast agents used in this study. The relaxivities of SPION did not change significantly after dye conjugation (Table 1). Carboxyl stabilized HTIO15 had the highest R2 value and R2/R1 ratios compared to the other SPION evaluated due to the core iron oxide crystal clustering and the particle size. The elevated R2 relaxivity of all the SPION evaluated results from either restricted water diffusion in thick hydrophilic polymers or by clustering of the nanoparticles.

3.2. Complex formation

The surface charge and type of SPION determines the complex formation. We maintained the similar complexation conditions ferumoxides (FE) and protamine sulfate (Pro, zeta potential 7.07±0.01 mV) for the FL SPION. Fixing the concentration of FL SPION and varying amounts of Pro over 24 hours has provided the opportunity to investigate the complex formation of FL SPION-Pro (Figure 1). The photographs of Texas HTIO10-Pro and Texas HTIO15-Pro indicate that the FL SPION-Pro complexes precipitate out of the solution at different ratios. Interestingly, when excess protamine sulfate is present in solution, the FL SPION-Pro complexes are stabilized and the nanoparticles do not precipitate out in aqueous solution. These finding are consistent with the previous results [14].

We also found that complexation conditions in culture media depended on the ionic strength and pH of the media, along with the polarity of FL SPION. By controlling surface properties, size and zeta potential of the SPION, we could predict the conditions for complexation that results in precipitation (see Figure 1c). Figure 1c shows a graph of the relationship of the protamine sulfate concentration to 100 μg/ml FL SPION and the parameter J for conditions that result in precipitation of the FL SPION-Pro complexes. The results show a linear relationship with good correlation between the concentration of protamine sulfate in media and the formation of FL SPION-Pro complexes with the parameter J equal to the slope that correlates to the hydrodynamic diameter of the transfection agent (shown in Figure 1c). This observation indicates that the theoretical assumptions can be used to predict the complex formation. The linear relationship suggests that larger size FL SPION are better for inducing

complexation with low concentrations of protamine sulfate. Solutions of FL-SPION and transfection agents show that as a result of complexation, precipitation occurs at zeta potentials approximately equal to zero, that is consistent with our previous studies [8,14,22]. To enhance magnetic properties of magnetically labeled cells, SPION should be efficiently labeled via the complex formation. Endocytosis by the cell can be mediated by optimal size of self-assembled complex and charge of the complex. It is important to note that complex formation should serve as a basic guideline for incorporating SPION into cells although optimization of labeling protocol will still be required. Complex formation has been used in different applications such as gene delivery or protein delivery to improve intracellular uptake into endosomes. This study shows that it is possible to magnetically label stem cells when SPION and transfection agents are combined over a range of electrostatically assembled complexation conditions.

3.3. Cell labeling in vitro study

The average iron content per hMSC and HeLa cell was shown in Table 2. The cell labeling efficiency of Texas HTIO15-Pro demonstrated higher iron intracellular content compared to FE-Pro complexes. The higher uptake may arise from more efficient complexation of the HTIO15-Pro. Higher iron content in cells enables efficient stem cell tracking *in vivo*. Greater than 90% of Texas HTIO15-labeled hMSC were positive for intracellular iron by Prussian blue staining (Figure 2).

The labeling efficiency of FE-Pro labeled and Texas HTIO10-labeled hMSC was equally effective. In contrast, Prussian blue staining of control unlabeled hMSC did not detect the presence of iron. Cell labeling efficiency and the iron content per hMSC and HeLa cell were dependent on several factors: cell type, cell concentration, media, media supplements, ratio of SPION to Pro, the SPION concentration, and incubation time [8]. There were no significant differences in cell proliferation as measured by MTS between unlabeled, FE-Pro and Texas HTIO15-Pro labeled cells at different time intervals even though decrease albeit minimal was observed by Texas HTIO10-Pro (Figure 3).

Unlabeled and control FE-Pro labeled hMSC did not show any fluorescence (Figure 4). In contrast, Texas HTIO10 and Texas HTIO15 labeled hMSC exhibited strong intra-cytoplasmic fluorescence without evidence of incorporation of nanoparticles in the nucleus. Thus, fluorescent microscopy images confirmed the higher (i.e., as determined by iron content) cell labeling efficiency of Texas HTIO10 and 15 labeled hMSC. Figure 5 contains MRI gradient echo T2* weighted images at 3 Tesla of agar samples containing Texas HTIO15-Pro labeled hMSC, FE-Pro labeled hMSC or unlabeled hMSC. MRI of the labeled cells clearly demonstrates hypointense voxels originating from agar samples in comparison to the homogenous appearance of the agar containing unlabeled hMSC. Labeling cells with Texas HTIO15 resulted in a greater decrease in signal intensity on T2* weighted images corresponding to an increase in the R2* values originating from the labeled cells. Measurement of $R2^*_{cell}$ by MRI showed an excellent correlation r2 = 0.96 for statistical analysis with $R2^*_{complex}$ (= (R2 relaxivity of SPION at 3 Tesla) × (iron concentration in cells) × (cell concentration in a gel)) at 3 Tesla (Figure 5d, see also Supporting Information for HeLa cells). Of note, labeling cells with Texas HTIO15-Pro resulted in a greater intracellular iron concentration as measured by NMR relaxometry compared to unlabeled cells (Table 2). We observed a similar change in signal intensity on T2* weighted images from HTIO15-Pro labeled cells and cells labeled with FE-Pro or Texas HTIO10-Pro compared to unlabeled cells. The MRI signal intensity enhancement can be indicative of a larger $R2^*_{cell}$ value. We hypothesize that three parameters contribute the $R2^*_{cell}$ value: higher NMR relaxivities of SPION, higher iron concentration within endosomes in cells and higher cell density. These three parameters can be combined to determine $R2^*_{complex}$ value. Therefore, $R2^*_{complex}$ suggests that SPION with higher NMR relaxivities (e.g., manganese magnetic engineered iron

oxide nanoparticles [17]) can have less of a change in MRI signal intensity on T2* weighted images because of possibly decreased uptake of the SPION-peptide complex by the cell. Figure 5 is an example of how the above hypothesis can predict a $R2^*_{cell}$ value. Of note, higher NMR relaxivities of SPION can also effect larger $R2^*_{cell}$ value. This result comes from SPION-peptide complexes being sequestered in endosomes and maintaining the integrity of SPION inside cell. In addition, dissolving of the SPION coat will result in less iron oxide crystals being shielded from surrounding water and therefore increasing the surface area of the SPION and increasing the effective R2 and R2* [23]. However, some SPION, depending on the coating, can lose their integrity and then, only two parameters (iron concentration in cells and higher cell concentration) can contribute to $R2^*_{cell}$ value.

3.4. Detection limit of in vivo fluorescent imaging

SPION that have higher NMR relaxivities used to label cells can increase the ability to detect the cells *via* MRI. However, endogenous iron from hemorrhage or ferritin in tissues can have a similar appearance to SPION labeled cells on MRI and Prussian blue staining. Therefore, multimodal SPION conjugated with fluorescent tag was introduced to aid in the differentiation of SPION labeled cells and regions containing endogenous iron on histological examination. It is necessary to determine prior to use for cell tracking studies the detection limit of fluorescent SPION for *in vivo* fluorescent imaging studies. To determine this limit a variable thickness tissue model was used in combination with FL SPION to estimate the penetration depth that an optical signal could be detected. In this study, we constrained the possible 3-dimensional free dye diffusion that would occur following direct injection of the fluorochrome into tissues to a 2-dimensional radial diffusion model by placing FL SPION suspension in between tissue slices of various thickness (i.e., 2–15mm) (see Figure 6). Chicken breast was chosen for these studies because its opacity appeared similar to that of a nude mouse. For *in vitro* study, we synthesized several types of FL SPION and measured the detection limit of the agent as a function of depth from the tissue surface. FL SPION (50 μg Fe) solution was placed on a slice of the tissue phantom and subsequent sections were added on top to increase the depth of the fluorescent dye. Region of interest (ROI) measurements were obtained at various thicknesses of the tissues and normalized to the signal intensity over the control tissue. The normalized signal intensity decreased as the thickness of tissue increased (Figure 6b). The detection depth for the Texas SPION was limited to approximated 9.3 ± 0.5 mm at which point FL SPION loaded samples could not be distinguished from controls. In similar experiments, the detection depth for Alexa 488 dextran conjugated SPION was 4.9 ± 0.3 mm and for Cy5.5 dextran conjugated SPION 14.6 ± 0.7 mm. The results suggest that Texas Red fluorochrome can be used for cell trafficking studies in a superficial flank tumor model.

3.5. Stem cell tracking In vivo Study

In vivo MR and fluorescent imaging of mice with bilateral 1 cm flank tumors and corresponding histological examination of the tumors are shown Figure 7. The flank tumor injected with Texas HTIO15-Pro labeled hMSC mixed with C6 glioma cells clearly demonstrated significant decreases in signal intensity and bloom artifact on T2* weighted MRI. Fluorescent imaging demonstrated an increase in signal intensity originating from the tumor at 7 days. Although co-registration of the MRI to optical imaging could not be performed, it was clear from the overlay of the *in vivo* fluorescent imaging on the white light photograph that the signal was originating from the same location as on the MRI. Prussian blue staining showed multiple iron-positive hMSC in both tumors. However, the tumor injected with FE-Pro labeled hMSC mixed with C6 tumor cells only showed hypointensities on T2* weighted in MRI. No fluorescent signal was observed by optical imaging. For this experiment, we could not analyze NMR T2 or T2* relaxation time values at day 7 post implantation due to high SPION labeled cell concentration in both flank tumors. These results suggest that FL SPION labeled hMSC can be detected within a rapidly growing tumor for at least 7 days. Both *in vivo* fluorescent and

MR imaging clearly demonstrated that hMSC remained localized in flank tumors. Therefore, hMSC labeled with FL SPION-protamine sulfate was useful for identifying cells in the *in vitro* and *in vivo* studies.

4. Conclusions

In conclusion, FL SPION were prepared by a simple EDC/Sulfo-NHS conjugation approach with carboxy1 stabilized high temperature synthesized iron oxide nanoparticles (HTIO). Complexing FL SPION to protamine sulfate was successfully introduced to magnetically label cells based on a theoretical approach. Our theoretical approach of SPION-peptide complexes could provide guidelines for cell labeling and possibly predicting NMR relaxation properties of labeled cells *in vitro*. Magnetic labeling of cells with Texas HTIO15-Pro complexes provided greater changes in signal intensity on T2* weighted images of magnetically labeled cells compared to other SPION-Pro complexes. The stem cell tracking was monitored by magnetically labeled cells with high temperature synthesized SPION and fluorescent SPION *in vitro* and *in vivo* models. hMSC stays intact in frank tumors after 7 days holds promise for the detection of stem cells in tissue. The major finding of this study is the theoretical estimation of complex formation and determining the detection sensitivity of FL SPION labeled cells in model systems. The results in this study also showed the enhanced stem cell tracking possibilities by magnetically labeled cells with mono-disperse core HTIO SPION and fluorescent SPION as compared to labeling cells with ferumoxides. The developed FL SPION-protamine complex will be used for monitoring stem cell migration for cell therapy in the future.

Acknowledgement

This research was supported by the Intramural Research Program of the Clinical Center at the National Institutes of Health. The authors would like to acknowledge the help of Dr. Leapman for TEM analysis and Dr. E. Kay Jordan for her assistance in taking care of *in vivo* experimental studies.

References

1. Shah K. Cancer Biology & Therapy 2005;4:518–523. [PubMed: 15908803]
2. Modo M, Hoehn M, Bulte JWM. Molecular Imaging 2005;4:143–164. [PubMed: 16194447]
3. Rad AM, Arbab AS, Iskander ASM, Jiang Q, Soltanian-Zadeh H. J. Magn. Reson. Imaging 2007;26:366–374. [PubMed: 17623892]
4. Frank JA, Miller BR, Arbab AS, Zywicke HA, Jordan EK, Lewis BK, Bryant LH, Bulte JWM. Radiology 2003;228:480–487. [PubMed: 12819345]
5. Bulte JWM, Douglas T, Witwer B, Zhang SC, Strable E, Lewis BK, Zywicke H, Miller B, van Gelderen P, Moskowitz BM, Duncan ID, Frank JA. Nat. Biotechnol 2001;19:1141–1147. [PubMed: 11731783]
6. Josephson L, Tung CH, Moore A, Weissleder R. Bioconj. Chem 1999;10:186–191.
7. Kraitchman DL, Gilson WD, Lorenz CH. J. Magn. Reson. Imaging 2008;27:299–310. [PubMed: 18219684]
8. Arbab AS, Yocum GT, Kalish H, Jordan EK, Anderson SA, Khakoo AY, Read EJ, Frank JA. Blood 2004;104:1217–1223. [PubMed: 15100158]
9. Wu YJ, Muldoon LL, Varallyay C, Markwardt S, Jones RE, Neuwelt EA. American Journal of Physiology-Cell Physiology 2007;293:C1698–C1708. [PubMed: 17898131]
10. Josephson L, Kircher MF, Mahmood U, Tang Y, Weissleder R. Bioconj. Chem 2002;13:554–560.
11. Maxwell DJ, Bonde J, Hess DA, Hohm SA, Lahey R, Zhou P, Creer MH, Piwnica-Worms D, Nolta JA. Stem Cells 2008;26:517–524. [PubMed: 18055451]
12. Lu CW, Hung Y, Hsiao JK, Yao M, Chung TH, Lin YS, Wu SH, Hsu SC, Liu HM, Mou CY, Yang CS, Huang DM, Chen YC. Nano Lett 2007;7:149–154. [PubMed: 17212455]
13. Yoon TJ, Kim JS, Kim BG, Yu KN, Cho MH, Lee JK. Angew. Chem.Int. Ed 2005;44:1068–1071.

14. Lee JH, Schneider B, Jordan EK, Liu W, Frank JA. Adv. Mater 2008;20:2512–2516.
15. Frullano L, Meade TJ. J.Biol. Inorg. Chem 2007;12:939–949. [PubMed: 17659368]
16. Qin J, Laurent S, Jo YS, Roch A, Mikhaylova M, Bhujwalla ZM, Muller RN, Muhammed M. Adv. Mater 2007;19:1874–1878.
17. Lee JH, Huh YM, Jun Y, Seo J, Jang J, Song HT, Kim S, Cho EJ, Yoon HG, Suh JS, Cheon J. Nat. Med 2007;13:95–99. [PubMed: 17187073]
18. Hyeon T, Lee SS, Park J, Chung Y, Bin Na H. J.Am. Chem. Soc 2001;123:12798–12801. [PubMed: 11749537]
19. Berret JF, Schonbeck N, Gazeau F, El Kharrat D, Sandre O, Vacher A, Airiau M. J.Am. Chem. Soc 2006;128:1755–1761. [PubMed: 16448152]
20. Arbab AS, Liu W, Frank JA. Expert Review of Medical Devices 2006;3:427–439. [PubMed: 16866640]
21. Bulte JWM, Vymazal J, Brooks RA, Pierpaoli C, Frank JA. J.Magn. Reson.Imaging 1993;3:641–648. [PubMed: 8347958]
22. Kalish H, Arbab AS, Miller BR, Lewis BK, Zywicke HA, Bulte JWM, Bryant LH, Frank JA. Magn. Reson. Med 2003;50:275–282. [PubMed: 12876703]
23. Yocum GT, Wilson LB, Ashari P, Jordan EK, Frank JA, Arbab AS. Radiology 2005;235:547–552. [PubMed: 15858093]

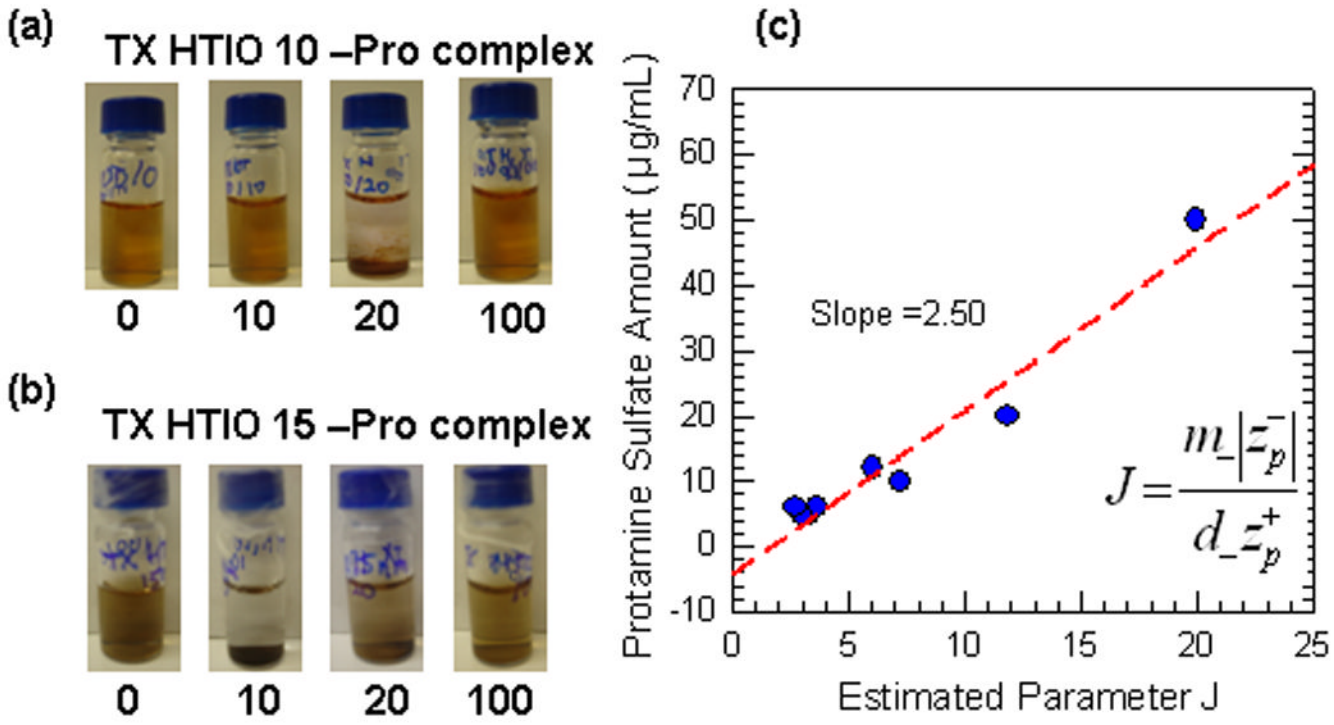

Figure 1.

Photographs of Texas HTIO10, 15-Pro complexes in water at different protamine sulfate concentrations with a fixed 100 µg/mL concentration of Fe (the number indicates protamine sulfate concentrations, unit µg/mL). (a) Texas HTIO10-Pro complexes; (b) Texas HTIO15 - Pro complexes; (c) Electrostatically assembled complexation - the relationship of the concentration of protamine sulfate to precipitate 100µg/mL Texas SPION and parameter J (unit = µg/nm), r2=0.98.

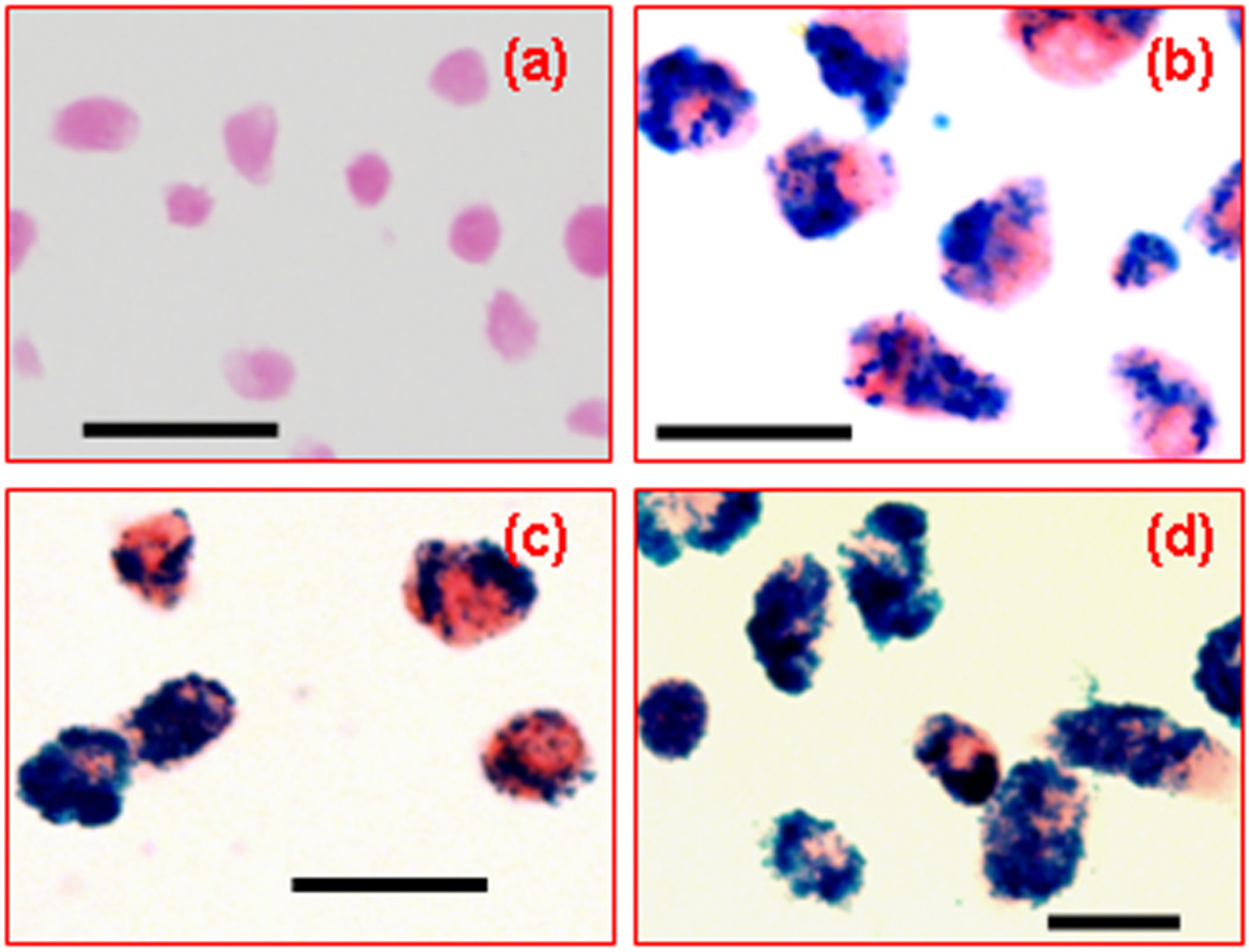

Figure 2.
Comparison of Prussian blue staining images with (a) control unlabeled hMSC; (b) FE-Pro labeled hMSC; (c) Texas HTIO10-Pro labeled hMSC; and (d) Texas HTIO15-Pro labeled hMSC. All nuclei were counterstained with nuclear fast red. Scale bar represents 50 μm.

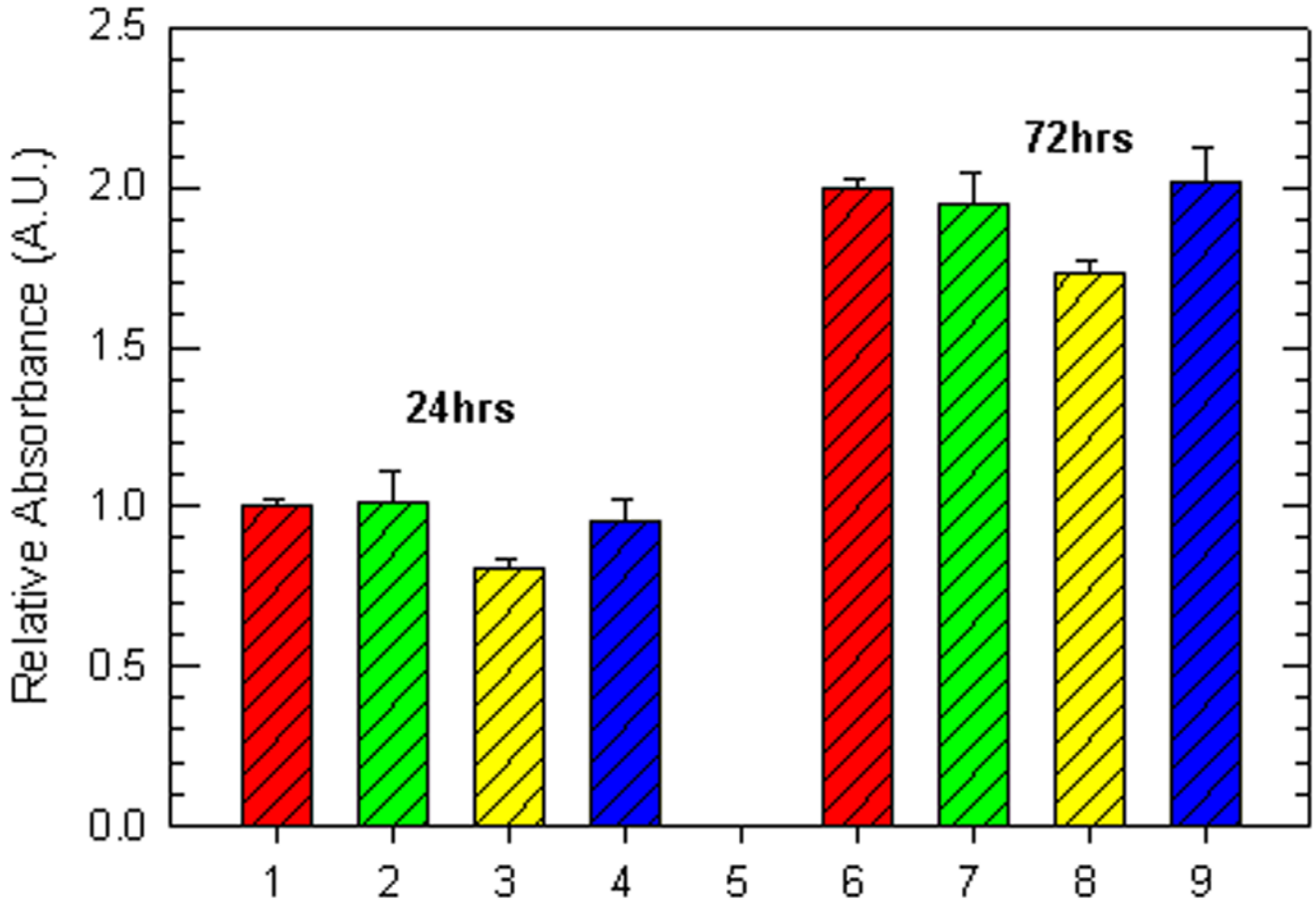

Figure 3.

MTS assay comparison of unlabeled hMSC (1,6); FE-Pro labeled hMSC (2,7); Texas HTIO10-Pro labeled hMSC (3, 8); and Texas HTIO15-Pro labeled hMSC (4, 9) after cells were grown in 96-well plates for 24 hours and 72 hours. The absorbance was measured at 490nm for proliferation and viability of cells, indicating no significant difference between Texas HTIO 15- Pro and unlabeled hMSC.

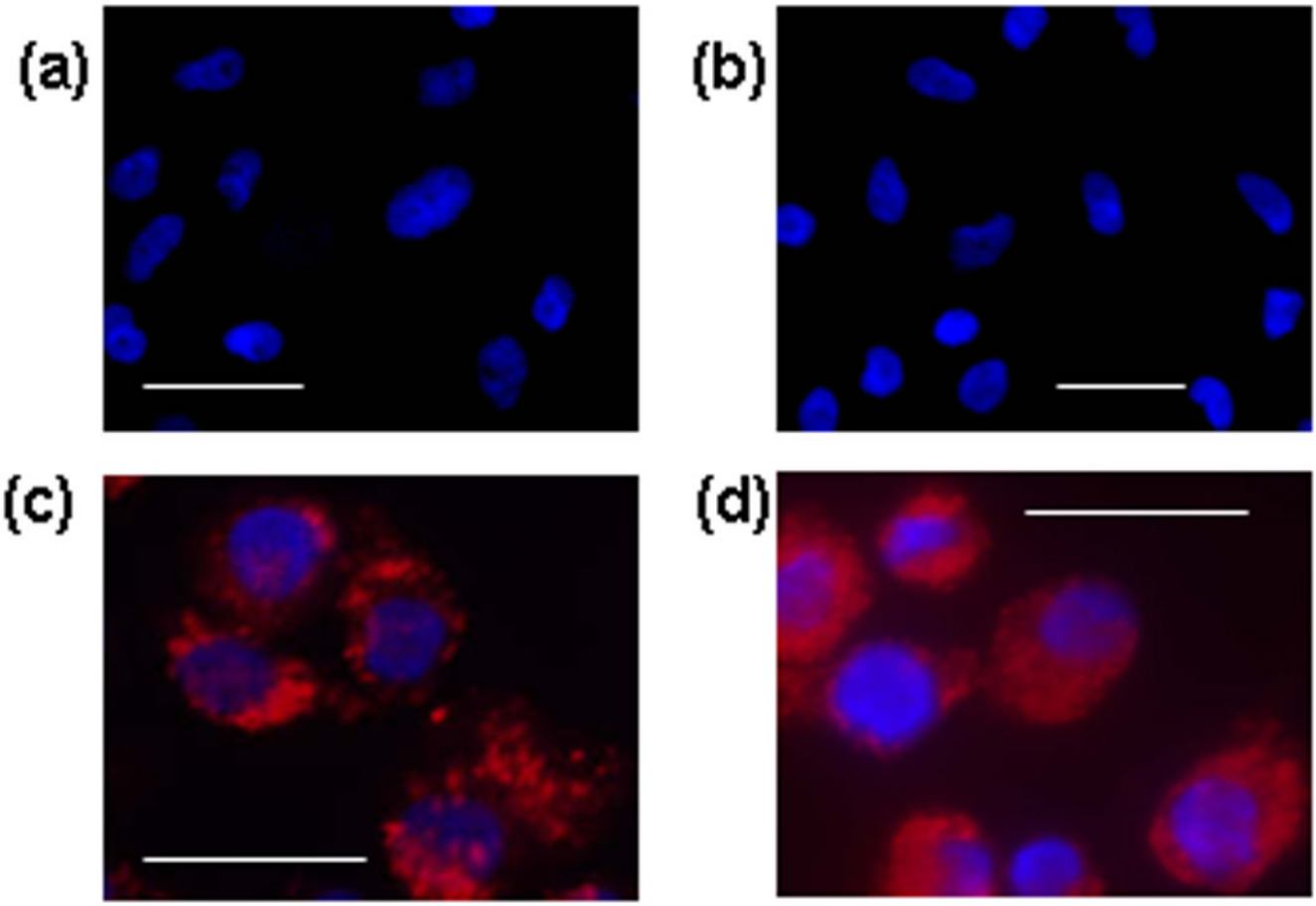

Figure 4.
Comparison of fluorescent microscopy images with (a) control unlabeled hMSC; (b) FE-Pro labeled hMSC; (c) Texas HTIO10-Pro labeled hMSC; and (d) Texas HTIO15-Pro labeled hMSC. All nuclei were labeled with DAPI. Scale bar represents 10um.

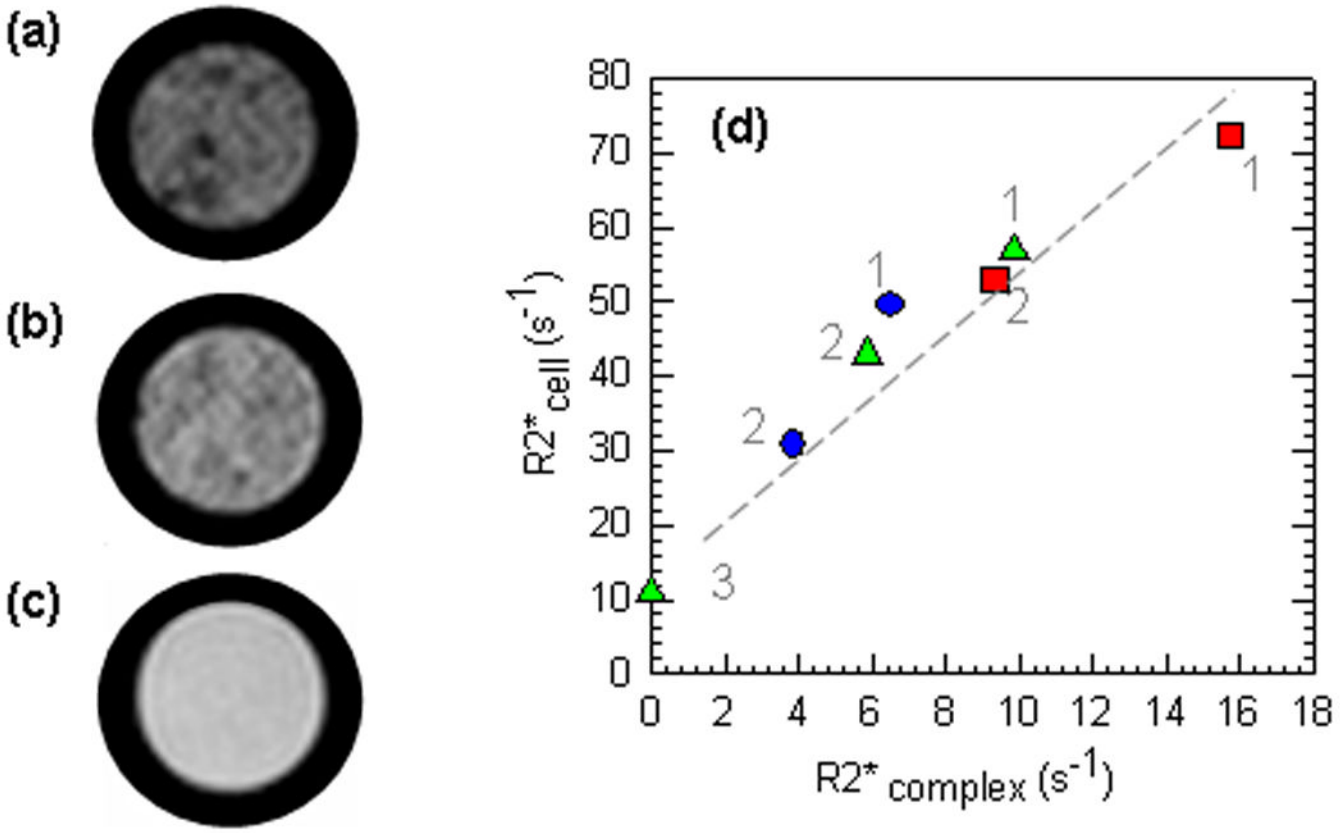

Figure 5.
T2* weighted sequence MR images from FL SPION-Pro complexes labeled hMSC suspended in an agar gel (8.3×10^4 cells/mL cell concentration). (a) Texas HTIO15-Pro labeled hMSC; (b) FE-Pro labeled hMSC; and (c) unlabeled hMSC. (d) Plot of R2* cell by MRI and R2* complex (=(R2* relaxivity of SPION in an agar gel at 3T) × (iron concentration in cell) × (cell concentration in a gel)), r2=0.96 (square, 2.0×10^5 cells/mL; triangle, 1.25×10^5 cells/mL; circle, 8.3×10^4 cells/mL; 1, Texas HTIO 15-Pro labeled hMSC; 2, FE-Pro labeled hMSC; 3, control unlabeled hMSC).

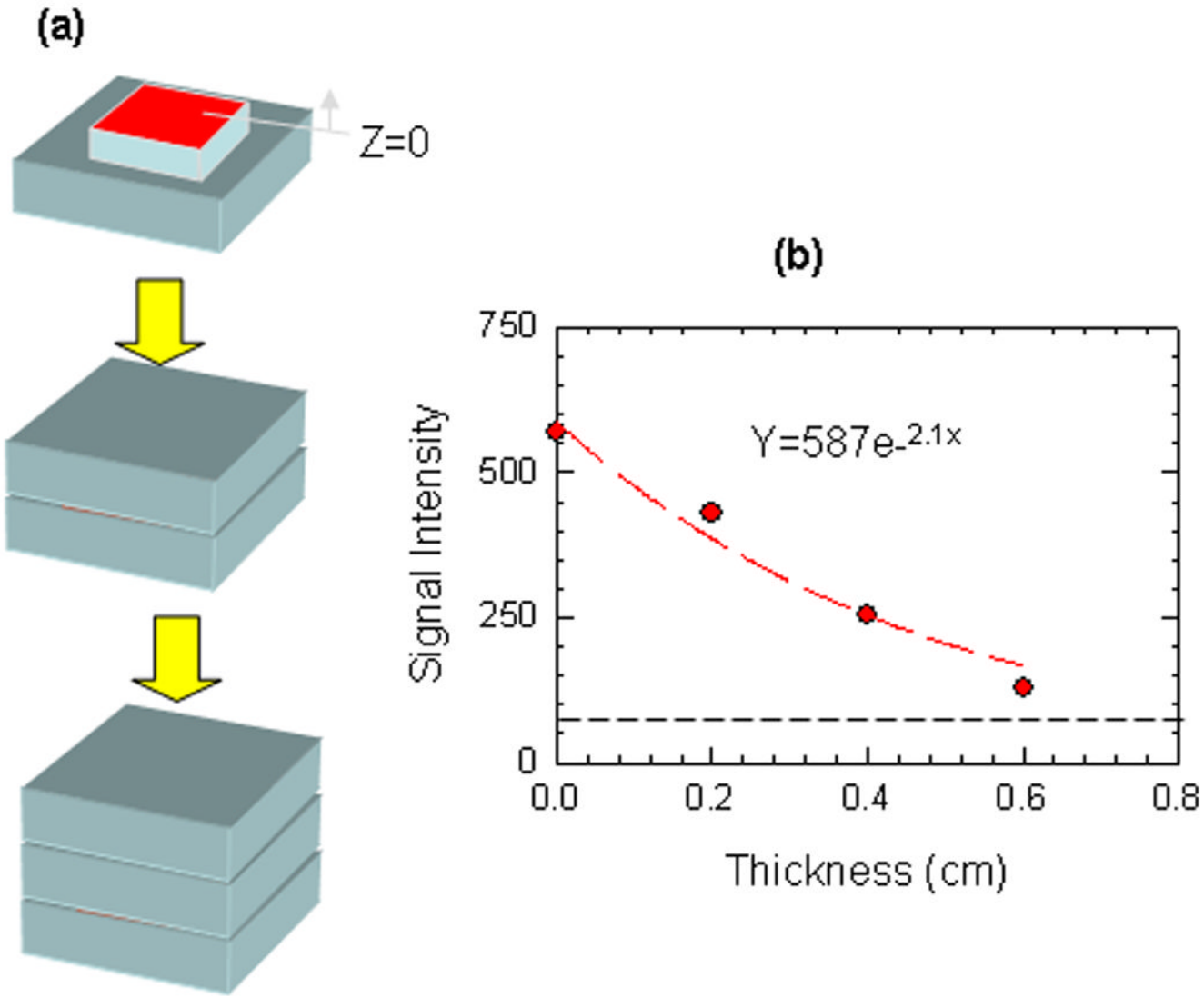

Figure 6.
(a) Chicken breast experimental phantom scheme for the detection limit of FL SPION. FL SPION (50ug) were loaded on the top of a section and then covered by tissues slices of various thicknesses in order to determine the ability to detect FL SPION. (b) The normalized signal intensity at various depths from the surface of the phantom compared to control sample (The dashed line represents the signal intensity of control tissue sample).

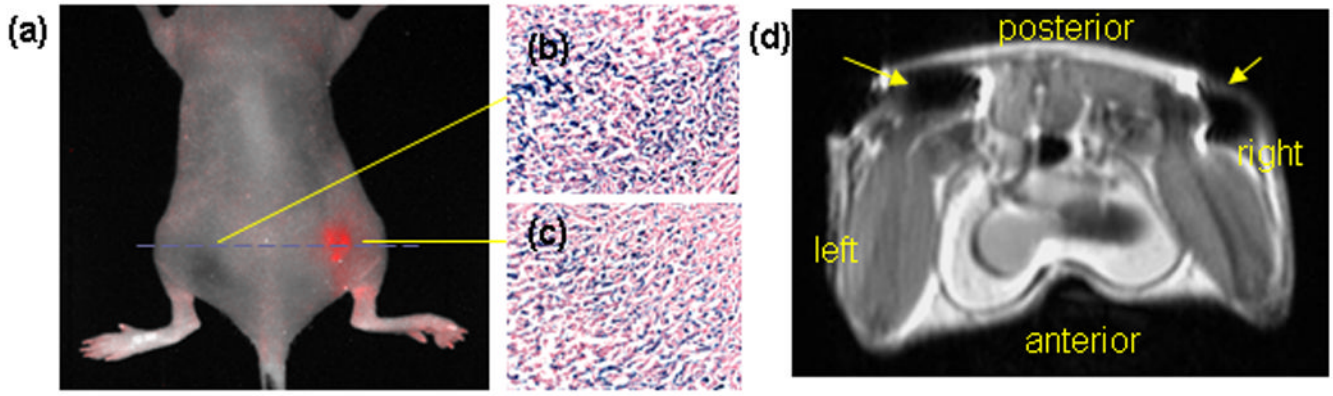

Figure 7.

(a) *In vivo* fluorescence imaging of subcutaneous flank tumor bearing mice 7days later after coinjection of Texas HTIO15-Pro labeled hMSC and unlabeled C6 gliomas (right side), and coinjection of FE-Pro labeled hMSC and unlabeled C6 gliomas (left side), the line represents the approximate MRI scanning line through the mouse, (b) histology of left side of flank tumor and (c) right side of flank tumor, (d) corresponding magnetic resonance image through a cross section slice of the mouse indicates hypointense (dark) voxels on right and left top sides (arrows) T2* images.

Table 1

Physico-chemical Properties of Texas Red SPIONs.

Sample	Hydrodynamic diameter (nm)	Zeta Potentials, mV	R_1[a] [$s^{-1}mM^{-1}$]	R_2[a] [$s^{-1}mM^{-1}$]	R_2/R_1	R_2*[b] [$s^{-1}mM^{-1}$]	CE (conj. Eff.)[c] (mmole/mole Fe)
Ferumoxides (FE)	157.3 ± 1.2	−32.6 ± 0.4	12.2	162.1	13.3	196.0	
HTIO (10nm)	31.2 ± 0.7	−14.7± 2.3	4.0	52.9	13.2		
Texas HTIO (10nm)	49.6± 0.1	−33.7± 3.6	5.0	83.6	16.5	100.3	1.1± 0.2
HTIO (15nm)	106.1 ± 0.7	−45.0 ± 2.3	8.3	200.3	24.2		
Texas HTIO (15nm)	101 ± 0.8	−50.8± 3.6	8.6	239.1	27.7	255.5	1.1± 0.2

[a] R1, R2 relaxivities at 1T

[b] R2* relaxivities at 3T

[c] CE: dye conjugation efficiency onto SPION (mmole dye /mole Fe)

Table 2

Iron Content and MR properties of labeled cells in gel.

Sample	Iron concentration in hMSC (pg/cell)	T_2*[a] [ms]	Iron concentration in HeLa cells (pg/cell)	T_2*[a] [ms]
Ferumoxides (FE)	13.3 ± 0.2	31.5±0.4	29.7 ± 0.2	19.9 ±0.4
Texas HTIO (10nm)	-		18.1 ± 0.1	25.7 ± 0.8
Texas HTIO (15nm)	17.2 ± 0.2	20.4±0.6	36.4 ± 0.3	8.2±0.2
Unlabeled	0.0 ± 0.1	94.5±2.6	0.1 ± 0.1	101.1±1.8

[a] cell concentration: 8.3×10^4 cells/mL